



**HAL**  
open science

## Full control of electric and magnetic light-matter interactions through a nanomirror on a near-field tip

Benoît Reynier, Eric Charron, Obren Markovic, Xingyu Yang, Bruno Gallas, Alban Ferrier, Sébastien Bidault, Mathieu Mivelle

### ► To cite this version:

Benoît Reynier, Eric Charron, Obren Markovic, Xingyu Yang, Bruno Gallas, et al.. Full control of electric and magnetic light-matter interactions through a nanomirror on a near-field tip. *Optica*, 2023, 10 (7), pp.841. 10.1364/OPTICA.486207. hal-04195064

**HAL Id: hal-04195064**

<https://hal.sorbonne-universite.fr/hal-04195064v1>

Submitted on 4 Sep 2023

**HAL** is a multi-disciplinary open access archive for the deposit and dissemination of scientific research documents, whether they are published or not. The documents may come from teaching and research institutions in France or abroad, or from public or private research centers.

L'archive ouverte pluridisciplinaire **HAL**, est destinée au dépôt et à la diffusion de documents scientifiques de niveau recherche, publiés ou non, émanant des établissements d'enseignement et de recherche français ou étrangers, des laboratoires publics ou privés.

1 **Full control of electric and magnetic light-matter**  
2 **interactions through a nanomirror on a near-field tip**

3 **BENOIT REYNIER,<sup>1</sup> ERIC CHARRON,<sup>1</sup> OBREN MARKOVIC,<sup>1</sup> XINGYU YANG,<sup>1</sup>**  
4 **BRUNO GALLAS,<sup>1</sup> ALBAN FERRIER,<sup>2,3</sup> SEBASTIEN BIDAULT<sup>4</sup> AND MATHIEU**  
5 **MIVELLE<sup>1\*</sup>**

6 <sup>1</sup> *Sorbonne Université, Centre National de la Recherche Scientifique, Institut des*  
7 *NanoSciences de Paris, 75005 Paris, France*

8 <sup>2</sup> *Chimie ParisTech, Paris Sciences & Lettres University, Centre National de la*  
9 *Recherche Scientifique, Institut de Recherche de Chimie Paris, 75005 Paris, France*

10 <sup>3</sup> *Faculté des Sciences et Ingénierie, Sorbonne Universités, UFR 933, Paris 75005,*  
11 *France*

12 <sup>4</sup> *Institut Langevin, ESPCI Paris, Université PSL, CNRS, 75005 Paris, France*

13 *\*[mathieu.mivelle@sorbonne-universite.fr](mailto:mathieu.mivelle@sorbonne-universite.fr)*

14 **Abstract:** Light-matter interactions are often considered governed by the electric  
15 optical field only, leaving aside the magnetic component of light. However, the  
16 magnetic part plays a determining role in many optical processes from light and chiral-  
17 matter interactions, photon-avalanching to forbidden photochemistry, making the  
18 manipulation of magnetic processes extremely relevant. Here, by creating a standing  
19 wave using a metallic nanomirror we manipulate the spatial distributions of the electric  
20 and magnetic fields and their associated local densities of states, allowing the selective  
21 control of the excitation and emission of electric and magnetic dipolar transitions. This  
22 control allows us to image, in 3D, the electric and magnetic nodes and anti-nodes of  
23 the fields' interference pattern. It also enables us to enhance specifically  
24 photoluminescence from quantum emitters excited only by the magnetic field, and to  
25 manipulate their spontaneous emission by acting on the excitation fields solely,  
26 demonstrating full control of magnetic and electric light-matter interactions.

27 © 2023 Optica Publishing Group under the terms of the [Optica Publishing Group Open Access Publishing](#)  
28 [Agreement](#)

29

## 30 **1. Introduction**

31

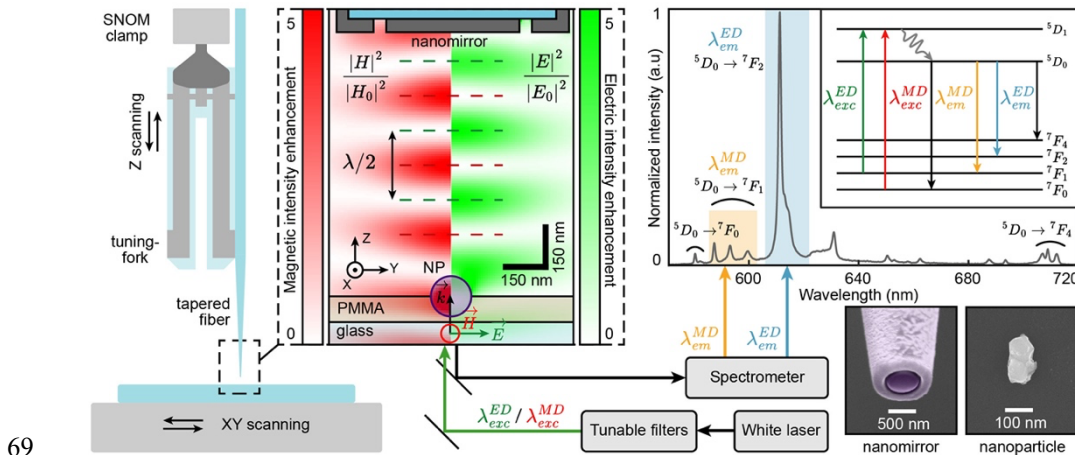
32 Manipulating light-matter interactions at the nanoscale has revolutionized many  
33 scientific fields. Whether it be in biology, with ever more sensitive diagnostics  
34 platforms [1, 2], medicine with targeted therapies [3, 4], chemistry with higher  
35 efficiency catalysis [5, 6], or physical optics with ever more exotic manipulations of  
36 these interactions [7-11]. Nevertheless, most of the systems developed to date have  
37 aimed at manipulating the electric component of light, leaving aside its magnetic  
38 counterpart. Indeed, light-matter interactions are often considered driven by the  
39 electric optical field alone, ignoring the magnetic component of light. However, this  
40 magnetic component plays a key role in many optical processes, such as chiral light-  
41 matter interactions [12], ultrasensitive detection [13], enhancement of Raman optical  
42 activity [14], photon-avalanching [15], or forbidden photochemistry [16], which  
43 makes the manipulation of magnetic processes extremely important. Over the past few  
44 years, several studies demonstrated a manipulation of specific ‘magnetic light’-matter  
45 interactions. For instance, luminescence mediated by magnetic transition dipoles was  
46 controlled and enhanced by manipulating the magnetic local density of states (LDOS)  
47 through metallic layers acting as mirrors [17-22] or with resonant dielectric [23-32]  
48 and plasmonic [33-36] nanostructures. It was also demonstrated that a Bessel beam  
49 could selectively excite a magnetic dipole transition through the magnetic field of light  
50 [37].

51 Here, we introduce a new platform made of a metallic nanomirror creating a standing  
52 wave pattern to manipulate the spatial distributions of the electric and magnetic fields  
53 and the associated LDOSes. With this platform, we demonstrate the selective  
54 excitation of electric (ED) or magnetic (MD) dipolar transitions and selectively collect  
55 the luminescence emitted by ED or MD transitions. This control allows us to image,  
56 in 3D, the electric and magnetic nodes and anti-nodes of the fields’ interference  
57 pattern. It also allows us to specifically enhance the luminescence of the quantum  
58 emitter by magnetic excitation only and to manipulate the spontaneous emission of the  
59 particle by acting on the excitation fields only, thus demonstrating total control of the  
60 magnetic and electric light-matter interactions.

61

62 **2. Results**

63 For this purpose, a metallic nano-antenna is fabricated at the tip of an aluminum-coated  
 64 tapered optical fiber (see Supplementary Materials 1) in a Scanning Near-Field Optical  
 65 Microscope (SNOM) and acts as a nanomirror when excited from the far-field to create  
 66 a standing wave (Fig. 1). This electromagnetic field is used to excite a  $\text{Eu}^{3+}$  doped  $\text{Y}_2\text{O}_3$   
 67 nanoparticle (see Supplementary Materials 1), whose position can be scanned at the  
 68 nanoscale in 3D under the SNOM tip, allowing a dynamic control of the interactions.



69 **Fig. 1.** Principle of the experiment. A metallic nanomirror fabricated at the tip of a tapered  
 70 fiber and placed on a SNOM (see Supplementary Materials 1) is brought near a  $\text{Y}_2\text{O}_3$   
 71 nanoparticle (NP) doped with  $\text{Eu}^{3+}$  ions. The excitation is performed by a spectrally  
 72 tunable laser and the luminescence signal is collected using a spectrometer. Numerical  
 73 simulations of the standing wave generated by the metallic nanomirror are displayed. The  
 74 interferences of the magnetic intensity of the standing wave at  $\lambda_{exc}^{MD}$  are on the left side, in  
 75 red, and those of the electric intensity at  $\lambda_{exc}^{ED}$  on the right side, in green. Both intensities  
 76 are normalized by the amplitude of the incident field. The dotted lines are guides for the  
 77 eye showing the spatial separation of the electric and magnetic anti-nodes in the standing  
 78 wave. The purple circle indicates the  $\text{Eu}^{3+}$ -doped particle. The emission spectrum (for  
 79 excitation at  $\lambda_{exc}^{ED}=532$  nm) of  $\text{Eu}^{3+}$  ions in the  $\text{Y}_2\text{O}_3$  matrix, with the magnetic and electric  
 80 transitions of interest highlighted respectively in yellow and blue, is represented (see  
 81 Supplementary Materials 1 for the emission spectrum when the particles are excited  
 82 through the magnetic transition at  $\lambda_{exc}^{MD}=527,5$  nm). The partial band diagram of  $\text{Eu}^{3+}$  ions  
 83 shows the electric ( $\lambda_{exc}^{ED}$ ) and magnetic ( $\lambda_{exc}^{MD}$ ) transitions at the excitation and, respectively,  
 84 at the emission ( $\lambda_{em}^{ED}$ ,  $\lambda_{em}^{MD}$ ).

86

87  $\text{Eu}^{3+}$  ions are known to exhibit pure electric and magnetic transitions in the visible  
88 spectrum, both in terms of excitation [37] and emission [18] (partial band diagram in  
89 the inset of Fig. 1). The excitation of the ED (at  $\lambda_{exc}^{ED} = 532$  nm) and MD (at  $\lambda_{exc}^{MD} =$   
90 527.5 nm) transitions is then performed by a white laser coupled to series of tunable  
91 filters, allowing the reduction of the laser spectrum to a bandwidth of only 2 nm. This  
92 bandwidth was chosen to minimize the crosstalk between electric and magnetic  
93 excitations according to the excitation spectrum of  $\text{Eu}^{3+}$  ions (see Fig. S1 in the  
94 Supplementary Materials). The luminescence of the ED (at  $\lambda_{em}^{ED} = 610$  nm) and MD  
95 (at  $\lambda_{em}^{MD} = 590$  nm) transitions of the  $\text{Eu}^{3+}$  ions is then collected by the same objective,  
96 filtered from the laser light, and measured by a spectrometer. The emission spectrum  
97 of europium ions is shown in Fig. 1. By tuning the position of the nanoparticle within  
98 the standing wave, we can thus selectively excite it with the E or H field and selectively  
99 collect the signal emitted by the ED and MD transitions. Therefore, we have access to  
100 the 3D distributions of the electromagnetic fields and of the local densities of optical  
101 states that act on the quantum emitters (i.e.  $\text{Eu}^{3+}$ ).

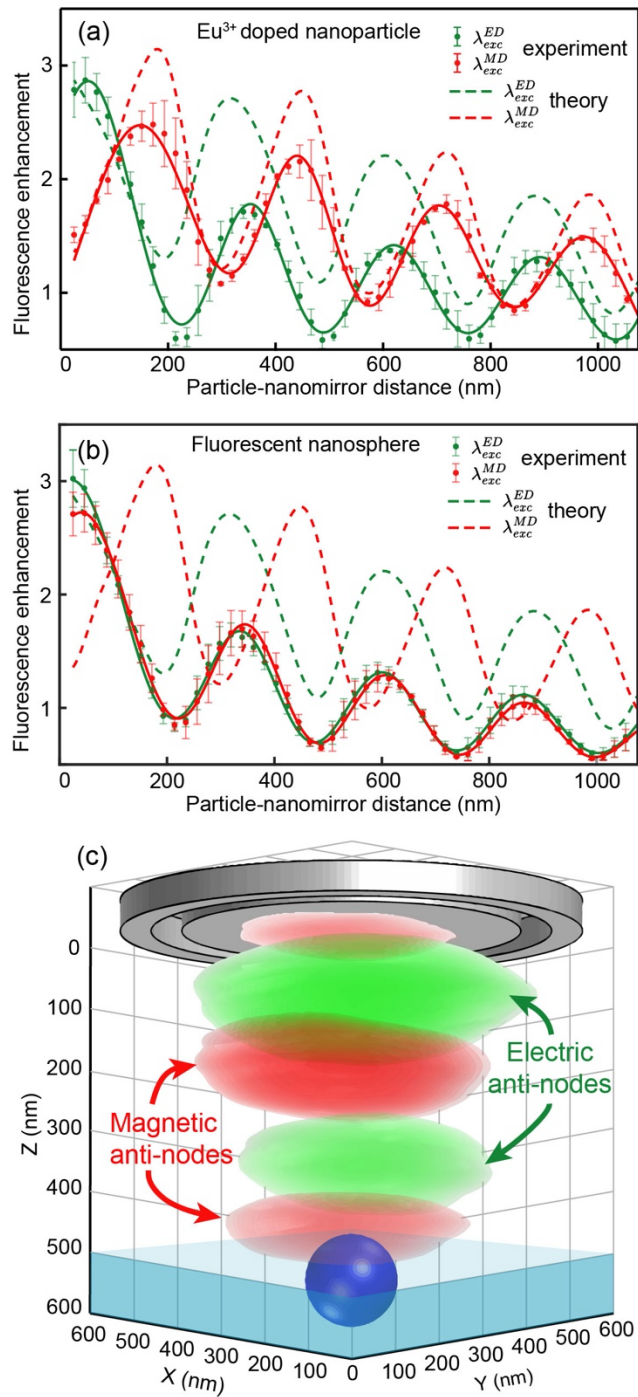
102 Fig. 1 shows the theoretical spatial distributions (see Supplementary Materials 2) of  
103 the electric and magnetic fields generated by the standing wave beneath the metallic  
104 nano-mirror at the  $\lambda_{exc}^{ED}$  and  $\lambda_{exc}^{MD}$  wavelengths, respectively. We observe that the  
105 electric and magnetic nodes and anti-nodes do not overlap spatially. A maximum E  
106 field corresponds to a minimum H field and vice versa. Furthermore, inside the anti-  
107 nodes, the field intensities are increased by a factor of five compared to the incident  
108 wave. Finally, due to the different continuity conditions at the interfaces, we can see  
109 that the two components of light do not penetrate the doped nanoparticle in the same  
110 way, with a clear predominance of the magnetic field inside the latter. Interestingly,  
111 this means that the E and H excitations take place at slightly different positions within  
112 the nanoparticle, as detailed further in the following paragraphs. Note that the  
113 amplitudes of the maxima of the electric and magnetic fields are due to the  
114 contributions of the reflection on the mirror, the gap between the nanodisc and the  
115 aluminum on the surface of the tip, the presence of the substrate, and the increase of  
116 the field within the particle. In particular, the presence of the particle and the substrate  
117 influence the amplitude of the standing wave but not the position of its nodes and anti-

118 nodes (see paragraph 2 of the Supplementary Materials for the field maps of these  
119 different conditions).

120 The luminescence intensity  $L$  of the europium-doped nanoparticle is proportional to  
121 the average excitation intensity within the nanoparticle according to the following  
122 equation:  $L = \sigma|A|^2\eta Q$ , where  $\sigma$  is the absorption cross-section,  $A$  is the electric or  
123 magnetic excitation field,  $\eta$  is the collection efficiency, and  $Q$  the quantum yield. Fig.  
124 2(a) provides the luminescence collected at  $\lambda_{em}^{ED}$  when exciting the particle at  $\lambda_{exc}^{ED}$  and  
125  $\lambda_{exc}^{MD}$  for different antenna-particle distances  $Z$  and normalized with respect to the  
126 luminescence intensities without the nanomirror. We observe that the signals do not  
127 overlap spatially: the maxima and minima for these two excitations are almost  
128 inversed, in excellent agreement with the theoretical results expected from the  
129 excitation of the particle by the E or H field of light (see paragraph 2 of the  
130 Supplementary Materials for different particle geometries). These measurements thus  
131 indicate that the evolution of  $L$  as a function of  $Z$  follows directly the evolution of the  
132 excitation probability and that  $Q$  and  $\eta$  have a negligible influence on the spatial  
133 distributions of the luminescence intensities. Importantly, since  $Q$  and  $\eta$  are  
134 independent of the nature of the excitation process (MD or ED) and only depend on  $Z$ ,  
135 it is possible to divide the luminescence enhancement measured at  $\lambda_{exc}^{ED}$  by the  
136 luminescence enhancement measured at  $\lambda_{exc}^{MD}$  and recover directly the ratio between  
137 the intensity enhancements of the E and H fields, providing a quantitative agreement  
138 between measurements and theory (see Fig. S2 in Supplementary Materials 1). These  
139 results also indicate that there is no spectral crosstalk between the two excitation  
140 channels. Although, it should be noted that even if  $Q$  and  $\eta$  do not influence the spatial  
141 distributions of the E and H fields, the difference in contrast between the theoretical  
142 and experimental curves in Fig. 2a,b can be explained by the fact that the experimental  
143 results, i.e., the number of photons collected, depend of the quantum yield of the  
144 dipoles and the collection efficiency of our system. These quantities are not considered  
145 in the theoretical results of Fig. 2a,b, which represent only the contributions of the  
146 electric and magnetic fields within the particle. Moreover, the shape of the particles  
147 can also influence this contrast (paragraph 2 of the Supplementary Materials).

148 As a control experiment, the measurement is also performed using a 200 nm diameter  
149 nanoparticle filled with fluorescent molecules (Fig. 2(b), see Supplementary Materials

150 1). In this case, magnetic transitions are negligible compared to their electrical  
151 counterpart, and the absorption spectrum overlaps with both the  $\lambda_{exc}^{ED}$  and  $\lambda_{exc}^{MD}$   
152 wavelengths (see Fig. S1 in Supplementary Materials 1). For fluorescent nanospheres,  
153 the curves are perfectly superimposed, and the signal follows a purely electric  
154 excitation. This measurement confirms that the luminescence collected in Fig. 2(a) for  
155 a  $\lambda_{exc}^{ED}$  excitation represents the spatial distribution of the E field intensity in the  
156 standing wave and that the signal for a  $\lambda_{exc}^{MD}$  excitation maps the magnetic field.  
157 Furthermore, we observe that the fluorescence intensity is enhanced by a factor of 3  
158 and 2.5 for, respectively, the excitation by the E and H fields compared to the signal  
159 collected without the antenna. This measurement provides the first demonstration of  
160 an enhanced luminescence signal from quantum emitters excited specifically by the  
161 magnetic component of light.  
162 Moreover, using the SNOM nano-positioning capabilities, the luminescence of  $\text{Eu}^{3+}$   
163 ions collected for each particle position in the volume under the nanomirror provides  
164 a 3D spatial reconstruction of the E and H field intensities of the standing wave as  
165 shown in Fig. 2(c). Here, the E and H nodes and anti-nodes are observed as lobes of  
166 the standing wave because of the nanoscale size of the metallic mirror. This is the first  
167 3D image providing, in parallel, the intensities of the electric and magnetic components  
168 of light.  
169  
170  
171



172

173 **Fig. 2.** Optical characterization of the standing wave. (a) Increase of the luminescence  
 174 intensities emitted by the  $\text{Eu}^{3+}$ -doped particle and collected by the spectrometer for  
 175 excitation wavelengths at  $\lambda_{exc}^{ED}$  (in green) and  $\lambda_{exc}^{MD}$  (in red) and for different  $Z$  positions of



176 the particle under the nanomirror. (b) Increase in fluorescence intensity emitted from  
 177 nanospheres filled with fluorescent molecules (see Supplementary Materials 1) for  
 178 different Z positions under the nanomirror and excited at  $\lambda_{exc}^{ED}$  (in green) and  $\lambda_{exc}^{MD}$  (in red).  
 179 In (a) and (b), the points correspond to the average values of the experimental data  
 180 normalized by the signal without the antenna, the solid curves are polynomial fits serving  
 181 as guides for the eye, and the dashed curves correspond to numerical calculations of the  
 182 expected signal for an excitation by the magnetic field, in red, or the electric field, in green,  
 183 of light. The error bars correspond to the standard deviation. (c) 3D image of the electric,  
 184 in green, and magnetic, in red, nodes and anti-nodes of the electromagnetic standing wave  
 185 generated under the nanomirror.

186

187 Finally, by tuning the excitation wavelength and studying separately the ED and MD  
 188 emission intensities, we study how the metallic nano-mirror modifies the spontaneous  
 189 emission rates for an electric or magnetic excitation. Since the emitted photons  
 190 originate from the same excited state, we can infer the  $\beta^{ED}$  and  $\beta^{MD}$  branching ratios  
 191 by considering any other transitions and non-radiative decay channels as losses [20]:

$$192 \quad \beta^{ED} = \frac{L^{ED}}{L^{ED} + L^{MD}} = 1 - \beta^{MD}, \quad (1)$$

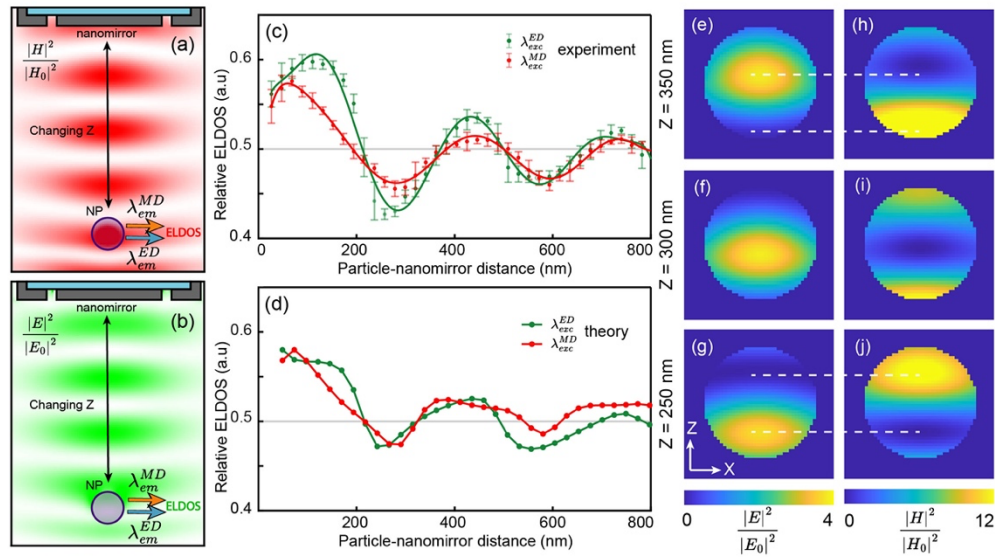
193 where  $L^{ED}$  and  $L^{MD}$  are respectively the luminescence signal emitted by the electric  
 194 and magnetic transitions.

195 It is then possible to determine the relative local densities of states experienced by the  
 196 ED (at  $\lambda_{em}^{ED}$ ) and MD (at  $\lambda_{em}^{MD}$ ) transitions as [20]:

$$197 \quad \tilde{\rho}^{ED} = \frac{\rho^{ED}}{\rho^{ED} + \rho^{MD}} = \frac{\beta_{NM}^{ED} / \beta_0^{ED}}{\beta_{NM}^{ED} / \beta_0^{ED} + \beta_{NM}^{MD} / \beta_0^{MD}} = 1 - \tilde{\rho}^{MD}, \quad (2)$$

198 with  $\beta_{NM}$  and  $\beta_0$  representing the branching ratios with and without nanomirror,  
 199 respectively. Fig. 3 provides the radiative electric LDOS when exciting the particle  
 200 using the E or H field, respectively, for different nanomirror-particle distances.  
 201 Interestingly, these two LDOSes, although measured at the same positions and thus in  
 202 the same photonic environment, do not overlap spatially. The explanation can be found  
 203 in the non-finite size of the  $\text{Eu}^{3+}$  doped nanoparticle. Indeed, depending on the  
 204 component of light that interacts with the particle, the position of the excited ions will  
 205 not spatially overlap because of a different spatial distribution of the fields within the  
 206 particle as shown in Fig. 3e-j (see paragraph 2 of the Supplementary Materials for

207 different particle geometries). The emitting ions will therefore be at different positions  
 208 corresponding to a different LDOS. Thus, by changing the nature of the exciting field,  
 209 it is possible to turn on or off some ions and probe different spatial distributions of the  
 210 LDOSes for electric and magnetic transition dipoles. These subtle variations are in  
 211 good agreement with theoretical calculations when the LDOS, inferred from the  
 212 photoluminescence measurements, is balanced by the distribution of the excitation  
 213 fields within the particle (Fig. 3e-j).



214

215 **Fig. 3.** LDOS change through field excitation. Principle of the experiment: The  
 216 nanoparticle is excited by a) the magnetic field (at  $\lambda_{exc}^{MD} = 527,5$  nm) or b) the electric field  
 217 (at  $\lambda_{exc}^{ED} = 532$  nm) for different mirror-particle distances. For each position, the number of  
 218 photons emitted through the electric (at  $\lambda_{em}^{ED} = 610$  nm) and magnetic (at  $\lambda_{em}^{MD} = 590$  nm)  
 219 channels are collected and used to calculate the relative Electric LDOS (ELDOS) via  
 220 equations 1 and 2. (c) Experimental and (d) Theoretical relative electric LDOS as a  
 221 function of the particle-nanomirror distance when the  $\text{Eu}^{3+}$  ions are excited at the resonance  
 222 wavelength of the magnetic dipole transition, in red, or the electric dipole transition, in  
 223 green. In (c) the solid curves are polynomial fits serving as guides for the eye and the error  
 224 bars correspond to the standard deviation;  $Z=0$  is chosen as the top part of the doped  
 225 particle. Theoretical distribution of (e-j) electric (at  $\lambda_{exc}^{ED}$ ) and (f-h) magnetic (at  $\lambda_{exc}^{MD}$ )  
 226 optical fields inside the nanoparticle, normalized by the incident wave and for different Z  
 227 positions of the particle under the nanomirror (indicated on the left side). A mask is applied

228 to remove the fields outside of the particle for clarity, and the diameter of the nanoparticle  
229 is 150 nm.

### 230 **3. Conclusion**

231 In conclusion, through a new platform, we demonstrated that by generating a standing  
232 wave with a nanomirror at the end of a SNOM tip, we could perfectly control the  
233 electric and magnetic interactions of light with quantum emitters, both in terms of the  
234 excitation probability and of the spontaneous decay channels. This manipulation  
235 allowed us to provide the first experimental 3D image of the electric and magnetic  
236 nodes and anti-nodes of a standing wave. Furthermore, we demonstrated an increase  
237 in the emission of a quantum emitter after specific excitation of its magnetic transition  
238 dipole, and we showed how, by this full control of the interactions, we could, in  
239 particular, manipulate the spontaneous emission of an emitter only by acting on the  
240 nature (magnetic or electric) its excitation. This research opens the way to many  
241 photonic applications involving a contribution from the optical magnetic field, such as  
242 chiral light-matter interactions [12], photochemistry [16], manipulation of magnetic  
243 processes [38], and new schemes in quantum computing [39] or nonlinear processes  
244 [15], among others.

245 **Funding.** Financial support from the Agence national de la Recherche (ANR-20-CE09-0031-  
246 01 and ANR-22-CE09-0027-04), from the Institut de Physique du CNRS (Tremplin@INP  
247 2020) and the China Scholarship Council.

248

249 **Author Contributions.** M.M supervised the study. B.R, E.C and O.M performed the  
250 experiments. B.R and X.Y performed the numerical study. A.F synthesised the Eu<sup>3+</sup>-doped  
251 nanoparticles. B.R, B.G, S.B and M.M analysed the data. All the authors discussed the results  
252 and contributed to writing the manuscript.

253

254 **Disclosures.** The authors declare no conflicts of interest.

255

256 **Data availability.** The data underlying the results presented in this paper are not publicly  
257 available at this time but may be obtained from the authors upon reasonable request.

258

259 **Supplemental document.** See Supplementary Materials for supporting content and methods.

260 **References**

261

- 262 1. D. Punj, M. Mivelle, S. B. Moparthi, T. S. van Zanten, H. Rigneault, N. F.  
263 van Hulst, M. F. García-Parajó, and J. Wenger, "A plasmonic 'antenna-in-box'  
264 platform for enhanced single-molecule analysis at micromolar concentrations," *Nat.*  
265 *Nanotechnol.* **8**, 512-516 (2013).
- 266 2. P. M. Winkler, R. Regmi, and V. Flauraud, "Antenna-based fluorescence  
267 correlation spectroscopy to probe the nanoscale dynamics of biological membranes,"  
268 *Nano. Lett.* **9**, 110-119 (2018).
- 269 3. D. P. O'Neal, L. R. Hirsch, N. J. Halas, J. D. Payne, and J. L. West, "Photo-  
270 thermal tumor ablation in mice using near infrared-absorbing nanoparticles," *Cancer*  
271 *letters* **209**, 171-176 (2004).
- 272 4. P. Fortina, L. J. Kricka, D. J. Graves, J. Park, T. Hyslop, F. Tam, N. Halas, S.  
273 Surrey, and S. A. Waldman, "Applications of nanoparticles to diagnostics and  
274 therapeutics in colorectal cancer," *Trends Biotechnol.* **25**, 145-152 (2007).
- 275 5. R. Grisel, K.-J. Weststrate, A. Gluhoi, and B. E. Nieuwenhuys, "Catalysis by  
276 gold nanoparticles," *Gold Bulletin* **35**, 39-45 (2002).
- 277 6. R. Sardar, A. M. Funston, P. Mulvaney, and R. W. Murray, "Gold  
278 nanoparticles: past, present, and future," *Langmuir* **25**, 13840-13851 (2009).
- 279 7. T. Taminiau, F. Stefani, F. Segerink, and N. Van Hulst, "Optical antennas  
280 direct single-molecule emission," *Nat. Photonics* **2**, 234-237 (2008).
- 281 8. M. L. Juan, M. Righini, and R. Quidant, "Plasmon nano-optical tweezers,"  
282 *Nat. Photonics* **5**, 349-356 (2011).
- 283 9. D. Akinwande, C. Huyghebaert, C.-H. Wang, M. I. Serna, S. Goossens, L.-J.  
284 Li, H.-S. P. Wong, and F. H. Koppens, "Graphene and two-dimensional materials for  
285 silicon technology," *Nature* **573**, 507-518 (2019).
- 286 10. J. J. Baumberg, J. Aizpurua, M. H. Mikkelsen, and D. R. Smith, "Extreme  
287 nanophotonics from ultrathin metallic gaps," *Nat. Mater.* **18**, 668-678 (2019).
- 288 11. B. Yang, G. Chen, A. Ghafoor, Y. Zhang, Y. Zhang, Y. Zhang, Y. Luo, J.  
289 Yang, V. Sandoghdar, and J. Aizpurua, "Sub-nanometre resolution in single-  
290 molecule photoluminescence imaging," *Nat. Photonics* **14**, 693-699 (2020).

- 291 12. Y. Tang and A. E. Cohen, "Optical chirality and its interaction with matter,"  
292 Phys. Rev. Lett. **104**, 163901 (2010).
- 293 13. Z. Xi and H. Urbach, "Magnetic Dipole Scattering from Metallic Nanowire  
294 for Ultrasensitive Deflection Sensing," Phys. Rev. Lett. **119**, 053902 (2017).
- 295 14. T. Wu, X. Zhang, R. Wang, and X. Zhang, "Strongly enhanced Raman  
296 optical activity in molecules by magnetic response of nanoparticles," J. Phys. Chem.  
297 C **120**, 14795-14804 (2016).
- 298 15. C. Lee, E. Z. Xu, Y. Liu, A. Teitelboim, K. Yao, A. Fernandez-Bravo, A. M.  
299 Kotulska, S. H. Nam, Y. D. Suh, and A. Bednarkiewicz, "Giant nonlinear optical  
300 responses from photon-avalanching nanoparticles," Nature **589**, 230-235 (2021).
- 301 16. A. Manjavacas, R. Fenollosa, I. Rodriguez, M. C. Jiménez, M. A. Miranda,  
302 and F. Meseguer, "Magnetic light and forbidden photochemistry: the case of singlet  
303 oxygen," Journal of Materials Chemistry C **5**, 11824-11831 (2017).
- 304 17. N. Noginova, Y. Barnakov, H. Li, and M. Noginov, "Effect of metallic  
305 surface on electric dipole and magnetic dipole emission transitions in Eu<sup>3+</sup> doped  
306 polymeric film," Opt. Express **17**, 10767-10772 (2009).
- 307 18. S. Karaveli and R. Zia, "Spectral tuning by selective enhancement of electric  
308 and magnetic dipole emission," Phys. Rev. Lett. **106**, 193004 (2011).
- 309 19. T. H. Taminiau, S. Karaveli, N. F. van Hulst, and R. Zia, "Quantifying the  
310 magnetic nature of light emission," Nat. Commun. **3**, 979 (2012).
- 311 20. L. Aigouy, A. Cazé, P. Gredin, M. Mortier, and R. Carminati, "Mapping and  
312 quantifying electric and magnetic dipole luminescence at the nanoscale," Phys. Rev.  
313 Lett. **113**, 076101 (2014).
- 314 21. R. Hussain, S. S. Kruk, C. E. Bonner, M. A. Noginov, I. Staude, Y. S.  
315 Kivshar, N. Noginova, and D. N. Neshev, "Enhancing Eu<sup>3+</sup> magnetic dipole  
316 emission by resonant plasmonic nanostructures," Opt. Lett. **40**, 1659-1662 (2015).
- 317 22. F. T. Rabouw, P. T. Prins, and D. J. Norris, "Europium-Doped NaYF<sub>4</sub>  
318 Nanocrystals as Probes for the Electric and Magnetic Local Density of Optical States  
319 throughout the Visible Spectral Range," Nano. Lett. **16**, 7254-7260 (2016).
- 320 23. B. Rolly, B. Bebey, S. Bidault, B. Stout, and N. Bonod, "Promoting magnetic  
321 dipolar transition in trivalent lanthanide ions with lossless Mie resonances," Phys.  
322 Rev. B **85**, 245432 (2012).

- 323 24. T. Feng, Y. Xu, Z. Liang, and W. Zhang, "All-dielectric hollow nanodisk for  
324 tailoring magnetic dipole emission," *Opt. Lett.* **41**, 5011-5014 (2016).
- 325 25. D. G. Baranov, R. S. Savelev, S. V. Li, A. E. Krasnok, and A. Alù,  
326 "Modifying magnetic dipole spontaneous emission with nanophotonic structures,"  
327 *Laser & Photonics Reviews* **11**, 1600268 (2017).
- 328 26. T. Feng, W. Zhang, Z. Liang, Y. Xu, and A. E. Miroshnichenko, "Isotropic  
329 magnetic Purcell effect," *ACS Photonics* **5**, 678-683 (2017).
- 330 27. M. Sanz-Paz, C. Ernandes, J. U. Esparza, G. W. Burr, N. F. van Hulst, A.  
331 Maitre, L. Aigouy, T. Gacoin, N. Bonod, M. F. Garcia-Parajo, S. Bidault, and M.  
332 Mivelle, "Enhancing magnetic light emission with all-dielectric optical  
333 nanoantennas," *Nano. Lett.* **18**, 3481-3487 (2018).
- 334 28. A. Vaskin, S. Mashhadi, M. Steinert, K. E. Chong, D. Keene, S. Nanz, A.  
335 Abass, E. Rusak, D.-Y. Choi, I. Fernandez-Corbaton, T. Pertsch, C. Rockstuhl, M. A.  
336 Noginov, Y. S. Kivshar, D. N. Neshev, N. Noginova, and I. Staude, "Manipulation of  
337 magnetic dipole emission from Eu<sup>3+</sup> with Mie-resonant dielectric metasurfaces,"  
338 *Nano. Lett.* **19**, 1015-1022 (2019).
- 339 29. P. R. Wiecha, C. Majorel, C. Girard, A. Arbouet, B. Masenelli, O. Boisron,  
340 A. Lecestre, G. Larrieu, V. Paillard, and A. Cuche, "Enhancement of electric and  
341 magnetic dipole transition of rare-earth-doped thin films tailored by high-index  
342 dielectric nanostructures," *Appl. Opt.* **58**, 1682-1690 (2019).
- 343 30. X. Cheng, X. Zhuo, R. Jiang, Z. G. Wang, J. Wang, and H. Q. Lin,  
344 "Electromagnetic Resonance-Modulated Magnetic Emission in Europium-Doped  
345 Sub-Micrometer Zirconia Spheres," *Advanced Optical Materials* **9**, 2002212 (2021).
- 346 31. H. Sugimoto and M. Fujii, "Magnetic Purcell enhancement by magnetic  
347 quadrupole resonance of dielectric nanosphere antenna," *ACS Photonics* **8**, 1794-  
348 1800 (2021).
- 349 32. Y. Brûlé, P. Wiecha, A. Cuche, V. Paillard, and G. C. des Francs, "Magnetic  
350 and electric Purcell factor control through geometry optimization of high index  
351 dielectric nanostructures," *Opt. Express* **30**, 20360-20372 (2022).
- 352 33. S. M. Hein and H. Giessen, "Tailoring Magnetic Dipole Emission with  
353 Plasmonic Split-Ring Resonators," *Phys. Rev. Lett.* **111**, 026803 (2013).

- 354 34. M. Mivelle, T. Grosjean, G. W. Burr, U. C. Fischer, and M. F. Garcia-Parajo,  
355 "Strong Modification of Magnetic Dipole Emission through Diabolo Nanoantennas,"  
356 ACS Photonics **2**, 1071-1076 (2015).
- 357 35. B. Choi, M. Iwanaga, Y. Sugimoto, K. Sakoda, and H. T. Miyazaki,  
358 "Selective Plasmonic Enhancement of Electric-and Magnetic-Dipole Radiations of Er  
359 Ions," Nano. Lett. **16**, 5191-5196 (2016).
- 360 36. C. Ernandes, H.-J. Lin, M. Mortier, P. Gredin, M. Mivelle, and L. Aigouy,  
361 "Exploring the magnetic and electric side of light through plasmonic nanocavities,"  
362 Nano. Lett. **18**, 5098-5103 (2018).
- 363 37. M. Kasperczyk, S. Person, D. Ananias, L. D. Carlos, and L. Novotny,  
364 "Excitation of magnetic dipole transitions at optical frequencies," Phys. Rev. Lett.  
365 **114**, 163903 (2015).
- 366 38. D. Bossini, V. I. Belotelov, A. K. Zvezdin, A. N. Kalish, and A. V. Kimel,  
367 "Magnetoplasmonics and femtosecond optomagnetism at the nanoscale," Acs  
368 Photonics **3**, 1385-1400 (2016).
- 369 39. D. Serrano, S. K. Kuppasamy, B. Heinrich, O. Fuhr, D. Hunger, M. Ruben,  
370 and P. Goldner, "Ultra-narrow optical linewidths in rare-earth molecular crystals,"  
371 Nature **603**, 241-246 (2022).
- 372  
373